CHAPTER 4

Glass transition temperature of metallic nanoparticles

4.1 Introduction

Metallic glasses have significant role in different fields of science due to their applications in small-scale devices, such as nano-electromechanical systems, biomedical implants, precision microparts, surgical tools, and micro machines [1].The first metallic glass was produced in 1960 by Duwez and coworkers by rapidly cooling a molten alloy of gold and silicon [2]. All metallic glasses are broadly classified into two categories: (i) the metal-metalloid glasses and (ii) the metal-metal glasses. One of the emerging classes of metallic glass is monoatomic metallic glass. However, the glassy behaviour of monoatomic metallic liquids is not yet efficiently explored. The liquid–glass transition phenomenon is observed in various types of liquids, such as molecular, ionic, metallic, oxide, and chalcogenide liquids [3-10]. Literature reveals that the verification of monoatomic metallic liquids is extremely difficult. However, Zhong et al. [11] achieved an unprecedentedly high quenching rate of 10^{14} K/s in nanoscale materials and vitrified the monoatomic metallic liquids on the extremely small nano-tips [11]. The verification of a super cooled liquid is often understood in terms of glass transition temperature (T_g) and the corresponding Kauzmann temperature (T_K). In a thermodynamic view of the glass transition, an ideal thermodynamic second-order transition should take place from a supercooled liquid to a glass with a single conformation at T_K [3-5,12,13]. The Kauzmann temperature represents a temperature, below which the transitional molecular motions responsible for major physical and chemical changes in materials can be negligible in the normal product timescales [14-16] and is always less than glass transition. As a result, T_K can be helpful to know the maximum temperature for storing the glasses. Previous studies shows that the T_g and T_K are size and dimension dependent thermodynamical parameters [12,17,18]. Theoretical as well as experimental methods have been employed to establish the relation between $T_g(D)$ and melting temperature $T_m(D)$[19,20]. Further, MD simulation has been employed to show that the $T_K(D)$of selected size will be lower than the bulk T_K [21].

However, due to kinetic restrictions it is difficult to measure direct experimental data for T_K. So, it can be indirectly determined by extrapolation from experimental data based on some theoretical models, such as the Vogel–Fulcher law with viscosity measurements [14,22,23] and Kauzmann [3]. The metallic nanoparticles such as silver (Ag), gold (Au), tantalum (Ta) etc. have special place in nanomaterial research due to the potential applications in digital circuits, biotechnology, and catalysts [24,25]. Particularly the Ta nanoparticles have significant applications in superconductors, orthopaedic implants dopants in photo electrode materials and micro-batteries [26]. Due to the difficulty in experimental setup, theoretical models as well as MD simulations can be used to evaluate the glass transition and Kauzmann temperatures. Theoretical models can be developed to evaluate these temperatures using cohesive energy expressions, due to linear relationship between them. Among them, number of cohesive energy models works for spherical nanoparticles only [27-30]. However, they cannot be used for any other shape except sphere or else, needs some modifications. Later on, few other models have been proposed, which accounts for both size and shape but they require lot of input parameters from literature or experimental work [31,32]. Due to lack of these data, the model adapts fitting parameters or approximations for the calculations [33].

4.2 Thermodynamics of size, shape and dimension on

4.2.1 Glass transition temperature (T_g)

In this work we have used expressions from chapter 2 to investigate size, shape and dimension dependent glass transition temperature (T_g) which is expressed as,

$$\frac{T_g(D)}{T_g(\infty)} = \left(1 - \frac{N}{2n}\right) \tag{4.1}$$

Where $T_g(D)$ and $T_g(\infty)$ represents glass transition temperature for size dependent nanoparticle and bulk material respectively. The related input parameters which is required for the calculations are given below.

Table 4.1: Comparison of N/ n values between Present model and Qi's model[34] for different shapes.

Shapes	Present model	Qi's model
Spherical	6h/ D	4h/ D
Cubic	6h/D	4h/D
Tetrahedral	14.7 h/D	9.79 h/D
Octahedral	7.38h/D	4.89h/D
Icosahedral	3.96 h/D	2.64 h/D
Cylindrical nanowire	4 h/D	2.66h/D
Thin films	2h/D	1.33h/D

Table 4.2: Input parameters for calculations [12,35]

Metallic nanoparticle	Atomic diameter h (nm)	$T_m(\infty)$ (K)	$T_g(\infty)$ (K)	$T_K(\infty)$ (K)
Ag	0.289	1235	750	333
Ta	0.292	3290	1754	888

It is clear from Fig.4.1 that glass transition temperature T_g of Ta nanoparticles decreases with decrease in size. The calculated values of present model are compared with MD simulation data [35] and Qi's model[34]. It is clearly observed from Fig.4.1 that our model is found more consistent than Qi's model with MD simulation data for D < 7nm. For D > 7 nm, deviation between calculated values and MD simulations is observed. Furthermore, we observe a rapid drop in glass transition temperature of Ta nanoparticles like Ag nanoparticles for D <7nm, due to increased surface-to-volume ratio. This indicates that the dynamics in the supercooled liquid region becomes much faster with decreasing size, in contrast to bulk liquids, liquid droplets with smaller sizes can only be frozen into glassy states in a much lower temperature region [35]. A major divergence in the curve between present work and Qi's model [34] is observed between size 3nm to 10nm in case of T_g. When the size of

nanomaterials decreases, several microscopic and quantum size effects dominates, such as the transformation of lattice structure and higher dissociation energies at the electronic shell-

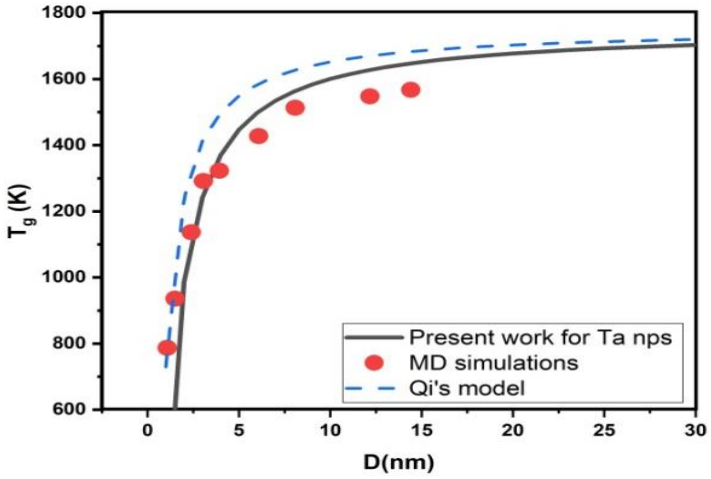

Figure 4.1: Size (D) dependent glass transition temperature (T_g) of tantalum nanoparticles.

closings [36]. As a result slight deviation is observed between our results and MD simulation data in the range <4nm because of ignorance of the quantum size effect and change in structure.

Fig. 4.2 depicts the glass transition temperature of Ta nanoparticles for different dimensions d=0, d=1, d=2. We found that the $T_g(d=0) < T_g(d=1) < T_g(d=2)$ for selected size of Ta nanoparticles within thermodynamical limit. Here thermodynamic limit reveals the range of size in which a prominent decrease in selected quantity can be observed. Further, the observed trend in the variation of T_g with different dimensions can be attributed to the atoms on the surface, edges and corners.

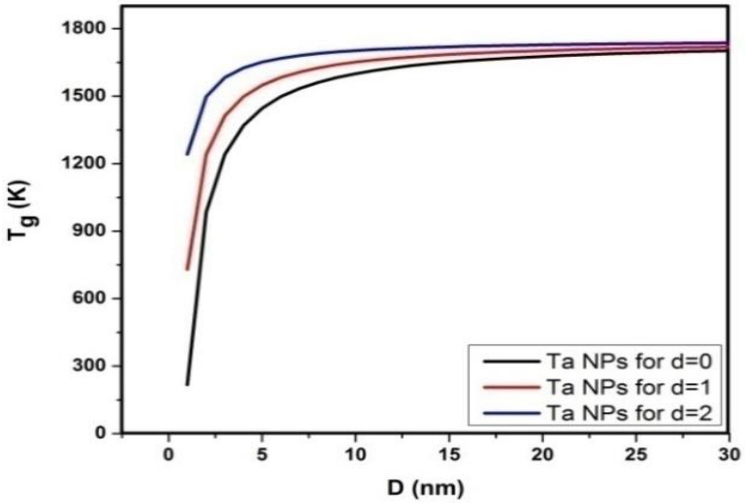

Figure 4.2: Size and dimension dependent glass transition temperature (T_g) of Ta nanoparticles.

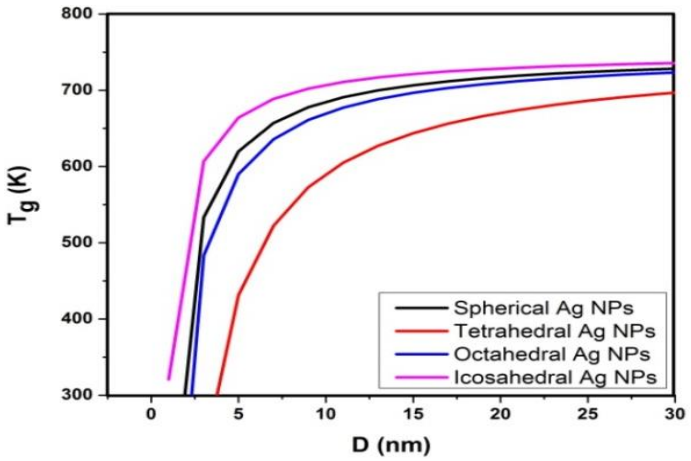

Figure 4.3: Size and shape dependent glass transition temperature (Tg) of Ag nanoparticles.

We now turn our attention to the variation in glass transition temperature for Ag nanoparticles of different shapes. Fig. 4.3 presents the variation of T_g with shape and size. In present work we have selected spherical, tetrahedral, octahedral and icosahedral shapes for study. It is observed that the icosahedral shaped Ag nanoparticle shows highest T_g and tetrahedral shaped Ag nanoparticle shows least T_g with constant size.

Fig. 4.4 shows the effect of size and dimensions on T_g of Ag nanoparticles using Equation 4.1. Due to difference in the values of N/n ratio for spherical (d=0), nanowire (d=1) and nano films (d=2) variation in the glass transition temperatures is observed. Table 4.1 clearly reveals that as N/n ratio of different dimensions decreases, T_g value of Ag nanoparticles increases with size.

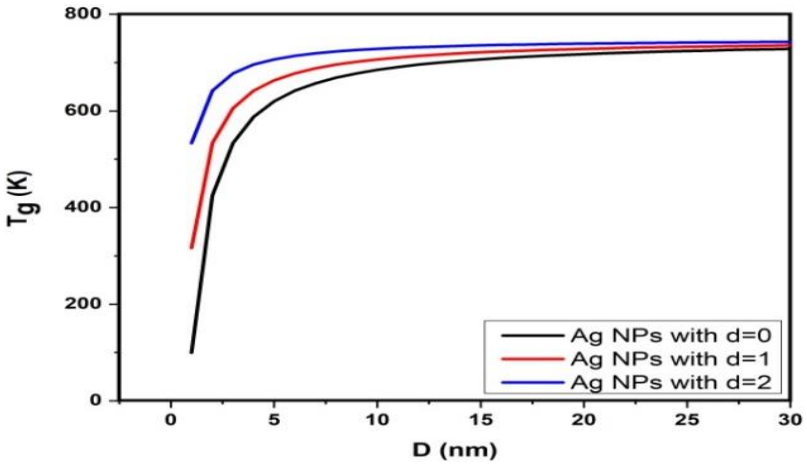

Figure 4.4: Size (D) and dimension (d) dependent glass transition temperature (T_g) of Ag nanoparticles.

4.2.2 Kauzmann temperature(T_K)

As T_K cannot be measured experimentally, we have obtained a relation between T_K and T_m(melting temperature) using Kauzmann theory. Moreover T_K is also called the entropy crisis temperature where entropy of liquid and its crystalline counterpart is the same [3].

$$S_m(T_K) = S_L(T_K) - S_S(T_K) = 0 \quad (4.2)$$

Where $S_m(T)$ denotes temperature dependent melting entropy, and the subscript m, L, and S represent the melting, liquid, and crystal transition, respectively. The Equation 4.2 can be modified using temperature-dependent Gibbs free energy difference between liquid and the crystal in bulk as given below which can be also experimentally verified as [12];

$$G_m(T,\infty) = \frac{7TH_m(\infty)[T_m(\infty)-T]}{T_m(\infty)[T_m(\infty)+6T]} \quad (4.3)$$

Here,$H_m(\infty)$ and$T_m(\infty)$ represent bulk melting enthalpy and bulk melting temperature. From Equation 4.3 we can predict that the $G_m(T,\infty)$ reaches its maximum value at T_K and when $dG_m(T,\infty)/dT_{T=T_K} = 0$. Thus we obtain Kauzmann temperature for bulk material as,

$$T_K(\infty) = [(\sqrt{7}-1)/6]T_m(\infty) \quad (4.4)$$

However, at nanoscale, Equation 4.3 can be written as [12],

$$G_m(T,D) = \frac{7TH_m(D)[T_m(D)-T]}{T_m(D)[T_m(D)+6T]} \quad (4.5)$$

The condition $dG_m(T, D)/dT_{T=T_K} = 0$ gives Kauzmann temperature with selected size as

$$T_K(D) = [(\sqrt{7}-1)/6]T_m(D) \quad (4.6)$$

Further, comparing Equation (4.4) and Equation (4.6) we get,

$$\frac{T_K(D)}{T_K(\infty)} = \frac{T_m(D)}{T_m(\infty)} \quad (4.7)$$

From our model we have, $\frac{T_m(D)}{T_m(\infty)} = \left(1 - \frac{N}{2n}\right)$ (4.8)

Thus using Equations 4.1, 4.7 and 4.8 we get the following expression;

$$\frac{T_m(D)}{T_m(\infty)} = \frac{T_K(D)}{T_K(\infty)} = \frac{T_g(D)}{T_g(\infty)} = \left(1 - \frac{N}{2n}\right) \qquad (4.9)$$

The Kauzmann and glass temperatures can be easily calculated for selected size, shape and dimension for selected material by using Equation 4.9. Using experimentally available bulk melting temperature, $T_K(\infty)$ can be calculated using Equation 4.4 while $T_g(\infty)$ is obtained from references[12,35].

Fig. 4.5 depicts the size dependent Kauzmann temperature calculated using Equation 4.9 for Ag nanoparticles. This figure also presents the data from MD simulation[12] and Qi's model [34]. The calculated values obtained using Equation 4.9 is found in better correspondence with the MD simulation results [12] than Qi's model[34] . This can be attributed to the introduction of critical diameter in the cohesive energy expressions. It is clearly seen from the Fig. 4.5 that the Kauzmann temperature decreases with decrease in size. Significant drop in T_K is seen for D <5 nm due to increased surface to volume ratio. As a result, when size increases, the value of Kauzmann temperature approaches towards bulk Kauzmann temperature. Further, the variation in Kauzmann temperature (T_K) with size for different dimension is calculated for Ag nanoparticles and presented in Fig. 4.6. It can be seen from Fig 4.6 that the T_K decreases with decrease in size as well as dimension. However, for the constant size the trend in T_K is observed as, $T_K(d=2) > T_K(d=1) > T_K(d=0)$. But this discrimination in T_K for different dimensions declines with increase in nanoscale size.

Our model predicts the value of $T_K(\infty)/T_m(\infty) \approx 0.27$ for Ag nanoparticles which is consistent with the value of 0.2–0.3 for metallic elements [12]. A size-independent T_K/T_m is interpreted with constant size effect on both T_K and T_m induced specifically by surface to volume ratio which also promotes that the intrinsic melting mechanism is independent of crystalline size and found consistent with Lindeman's melting criterion[12].

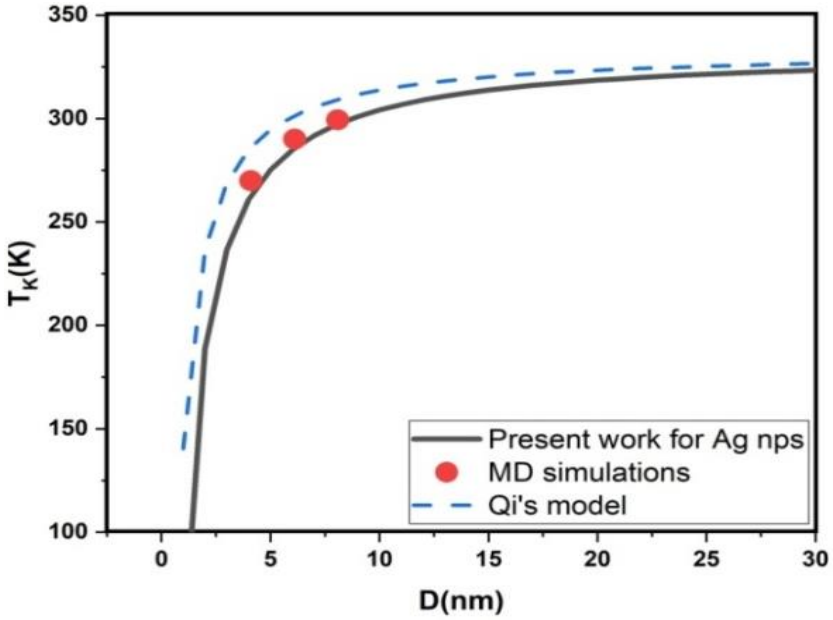

Figure 4.5: Size dependent Kauzmann temperature of spherical Ag nanoparticles.

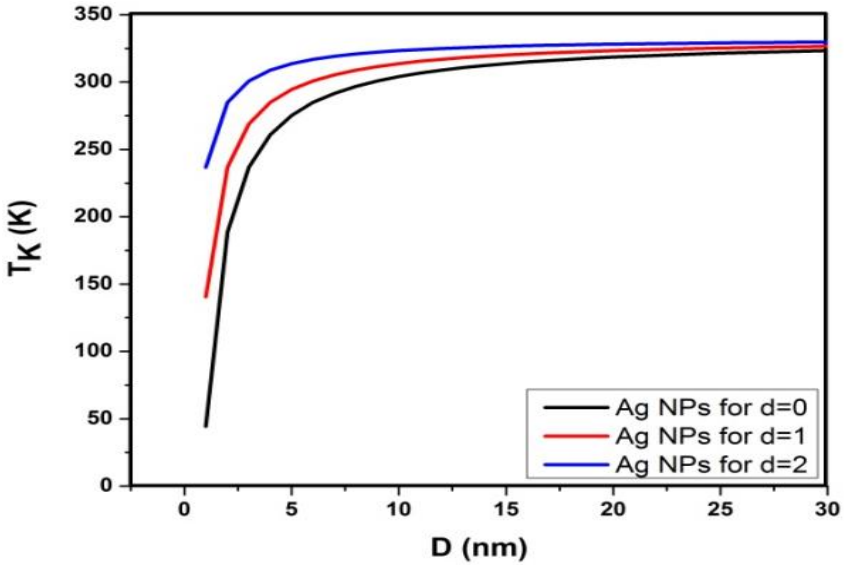

Figure 4.6: Size and dimension dependent Kauzmann temperature of Ag nanoparticles.

The variation in T_K with respect to size in terms of shapes and dimensions are presented in Fig. 4.7 and Fig 4.8. Here, Fig.4.7 clearly shows that the tetrahedral shape has least and icosahedral shape has highest value of T_K for selected size.

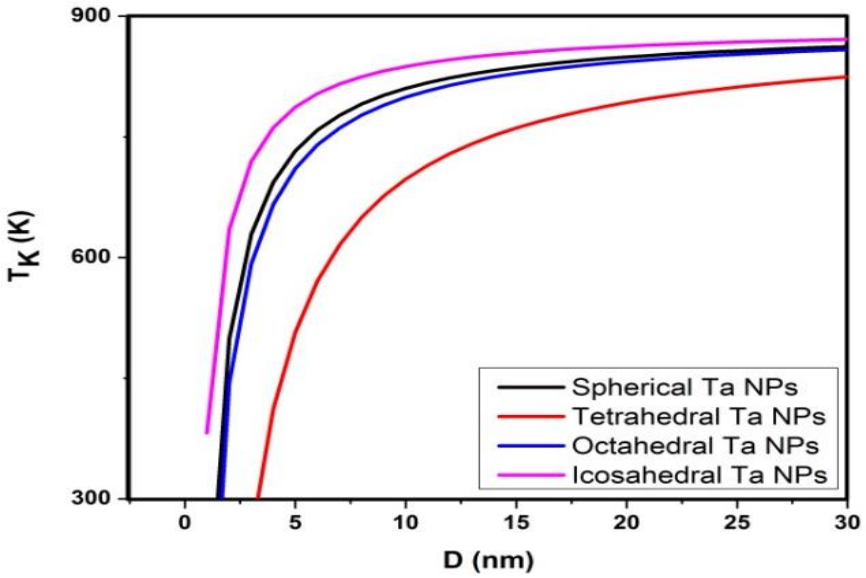

Figure 4.7: Size dependent Kauzmann temperature (T_K) of Ta nanoparticles

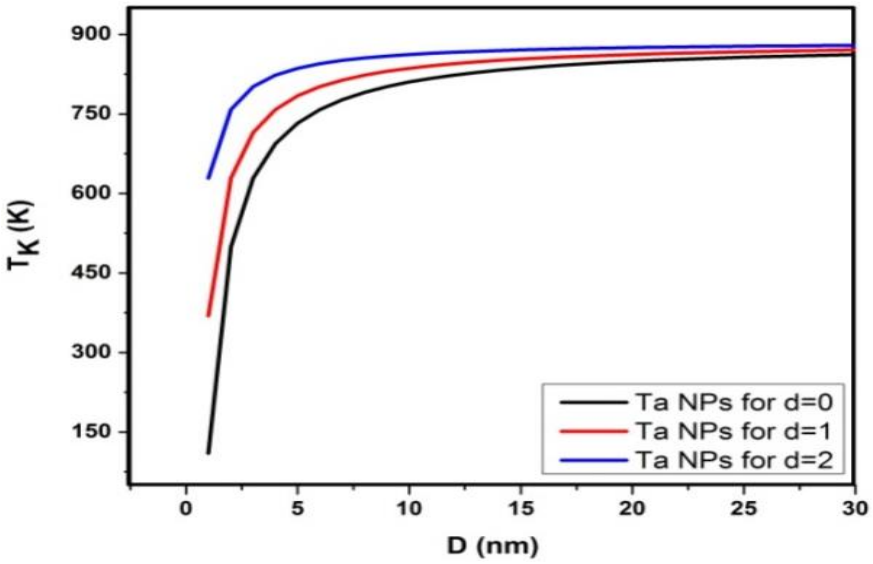

Figure 4.8: Size and dimension dependent Kauzmann temperature (T_K) of Ta nanoparticles

4.3 Relation between melting temperature, glass transition temperature and Kauzmann temperature

The glass transition temperature and the melting temperature are two most important factors to consider when processing polymers. At temperature above T_g but below T_m, there is a "rubbery region," where the material can exhibit large elongations under relatively low load [37].

Fig. 4.9 shows the variation in temperature of spherical Ag nanoparticles as a function of size (D) using Equation 4.9. Among the three temperatures, it is observed that $T_m(D)>T_g(D)>T_K(D)$ for the selected nanoparticle. The significant reason is, at the molecular level at Tg, the chains in amorphous (i.e., disordered) regions of the polymer gain enough thermal energy to begin sliding past one another at a noticeable rate while at the temperature where entire chain movement occurs is called the melting point (T_m) and is greater than the T_g. Below T_g, there exists disordered amorphous solid where chain motion is frozen and the temperature at which the difference in entropies becomes zero is Kaumann temperature. The more immobile the chain, the higher the value of T_g. While, below T_m it is an ordered crystalline solid which becomes disordered when melt above T_m. All three temperatures show similar characteristics and significant drop in temperatures for D<5 nm. This indicates that the dynamics in the supercooled liquid region becomes much faster with decreasing droplet size, so that in contrast to bulk liquids, liquid droplets with smaller sizes can only be frozen into glassy states in a much lower temperature region.

It is observed from Fig. 4.10 that temperatures for Ta nanoparticles vary with size (D). All the three temperatures for Ta nanoparticles are found in close proximity for D =1 nm, but as the size increases the temperatures diverges from each other. Glass transition temperature of Ta nanoparticles are found intermediate among melting and Kauzmann temperatures. This graph can be a helpful tool to compare the melting, Kauzmann and glass transition temperature.

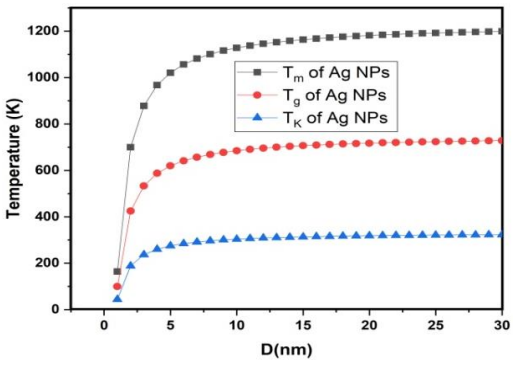

Figure 4.9: Variation in melting, glass transition and kauzmann temperature of Ag nanoparticles as a function of size (D)

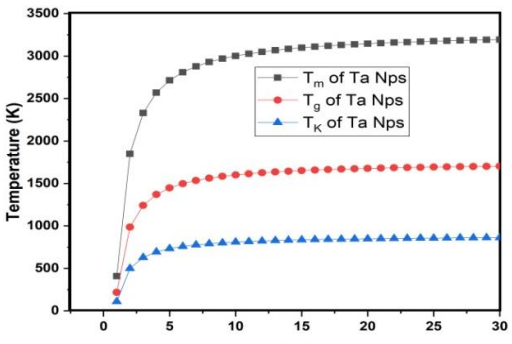

Figure 4.10: Variation in melting, glass transition and kauzmann temperature of Ta nanoparticles as a function of size (D)

4.4 Comparison of surface to volume ratio of atoms for different shapes with size

We have observed in the previous graphs that temperatures vary due to change in shapes, sizes and dimensions. In our model shape factor is N/n ratio, from that we have selected N_1/n_1 (which is also known as surface to volume ratio) because it ultimately provides the number of atoms present in the prescribed shape at definite size.

Table 4.3: Values of N_1/n_1 for different shapes.

Shapes	N_1/n_1
Tetrahedral	9.78h/D
Octahedral	4.91h/D
Icosahedral	2.64h/D
Spherical	4h/D
Nanowire	2.66h/D
Thin film	0.66h/D

Here h/D is the ratio of atomic diameter to the selected diameter/length/thickness of the nanoparticle. This ratio varies from selected material to material.

Fig. 4.11 demonstrates surface to volume ratio of atoms (N_1/n_1) for icosahedral, spherical, octahedral and tetrahedral shapes with inverse diameter (D^{-1}) for Ag and Ta nanoparticles. All the values of N_1/n_1 are obtained from Table 4.3 and the detail formulation is mentioned in chapter 2. Among the selected shapes, icosahedral, spherical and octahedral are seen in close vicinity while tetrahedral shaped nanoparticles are observed at distant position with reference to rest of the shapes. Hence it is clear that (N_1/n_1) (tetrahedral)>(N_1/n_1)(octahedral)> (N_1/n_1)(spherical)>(N_1/n_1)(icosahedral) for constant nanosize of Ag and Ta nanoparticles. As ratio of atoms for tetrahedral shape is highest which in turn shows maximum availability of atoms on surface and thus results into least melting, glass transition and Kauzmann temperatures among other shapes for selected nanosize[38]. In case of different shaped nanoparticles, prominent ratio of surface to volume atoms can be seen for D^{-1}> 0.2 nm^{-1} or D<5 nm for both materials. Beyond this size, the ratio of atoms gradually approaches to the constant value irrespective of selected shape and material.

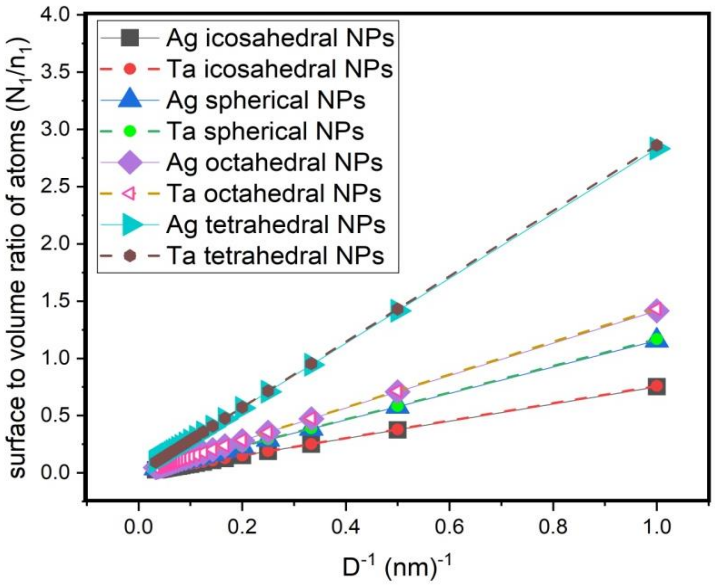

Figure 4.11: Comparison of surface to volume ratio of atoms (N_1/n_1) for different shapes with inverse size (D^{-1}) for Ag and Ta NPs.

Fig. 4.12 presents the dimension dependent surface to volume ratio of atoms for Ag and Ta nanoparticles. We observe that, surface to volume ratio of atoms follows the sequence as (N_1/n_1)(nanosphere)>(N_1/n_1)(nanowire)> (N_1/n_1) (nanofilm) for Ag and Ta nano particles within nanoscale, which in turn demonstrates the highest availability of atoms on surface for nano sphere(0-d).

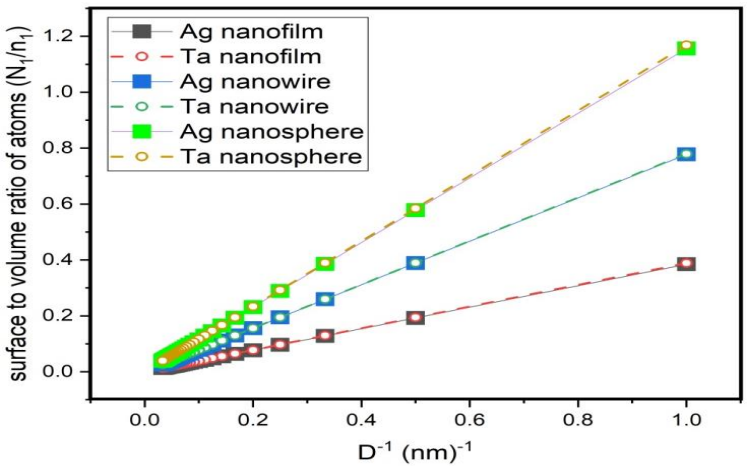

Figure 4.12: Comparison of surface to volume ratio of atoms (N_1/n_1) for different dimensions with inverse size (D^{-1}) for Ag and Ta NPs.

Hence results into least glass transition and Kauzmann temperatures among other dimensions and can be confirmed from Fig. 4.2, 4.4, 4.6 and 4.8 for both Ag and Ta nanoparticles. The ratio of atoms nearly coincides for Ag and Ta nanoparticles for selected size, shape and dimension on the basis of close proximity in their atomic diameter with a difference of ≈ 0.003 nm and is evident from Fig. 4.11 and 4.12.

4.5 Conclusions

Based on the above analysis, it is clear that the atoms on the surface layer possess much faster dynamics than those in the interior of selected shaped nanoparticles [35]. As a result with decreasing size, the surface layer plays more and more important roles in the dynamical and mechanical properties of the nanoparticles.

During the investigation we found that temperatures decrease with decrease in size (D) due to increased surface to volume ratio. Our model predictions showed good agreement with the available molecular dynamical data in both the cases of $T_g(D)$ and $T_K(D)$. For selected nanosize, shape and dimension we observed the series of temperatures as $T_m(D) > T_g(D) > T_K(D)$. In case of d=0; both glass transition and Kauzmann temperature follows the sequence as; (icosahedral,D) >(spherical,D) >(octahedral,D) >(tetrahedral,D) for selected nanoparticle. While in terms of dimensions, they follow sequence as $d=0 < d=1 < d=2$ for selected size and metallic nanoparticle. These results are obtained on the ground of surface to volume ratio, which in turn shows the availability of atoms on surface. Higher surface to volume ratio will result into least melting temperatures within nanosize. Thus we conclude that shape and dimension can be effective only within thermodynamic limit of few nanometers and gradually the impact of these parameters on any thermodynamical properties declines with increase in size. These conclusions can be fruitful for potentially manipulating the properties of metallic liquids and glasses within scale of nanometer.

References

1. G. Kumar, A. Desai, and J. Schroers, *Advanced Materials.* **23**, 461 (2011).
2. M. M. Khan, A. Nemati, Z. U. Rahman, U. H. Shah, H. Asgar and W. Haider, *Critical Reviews In Solid State and Materials Sciences.* **43**, 233 (2017).
3. W. Kauzmann, *Chem. Rev.* **43**, 219 (1948).

4. P. G. Debenedetti and F.H. Stillinger, *Nature*. **410**, 259 (2001).
5. J. H. Gibbs and E.A. Di Marzio , *J. Chem. Phys.* **28**, 373 (1958).
6. S. Sastry, P.G. Debenedetti and F.H. Stillinger, *Nature.* **393**, 554 (1998).
7. V. Krakoviack, *Phys. Rev. Lett.* **94**, 065703, (2005).
8. A. Scala, F. W. Starr, E.L. Nave, F. Sciortino and H.E. Stanley, Nature. 406,166-175 (2000).
9. S. Sastry, Nature. 409,164 (2001).
10. H. Tanaka, *J. Non-Cryst. Solids.* **351**, 3396 (2005).
11. L. Zhong, et al., *Nature*. **512**,177 (2014).
12. Ao. Z. M. Zheng and W.T. Jiang Q., *Nanotechnology.* **18**, 255706 (2007).
13. G. Adam and J.H. Gibbs, *J. Chem. Phys.* **43**, 139 (1965).
14. Q. Jiang, M. Zhao and X.Y. Xu, *Phil. Mag. B.* **76**, 1 (1997).
15. F.H. Stillinger, et al. *J. Phys. Chem. B.* **103**, 7390 (1999).
16. B. Coluzzi, G. Parisi and P. Verrocchio, *Phys. Rev. Lett.* **84**, 306 (2000).
17. S. Mishra, P.K. Jha, A. Pratap, *J Therm Anal Calorim.* **107**, 65 (2012).
18. P. A. Bhatt, A. Pratap, P.K. Jha, *J of thermal analysis and calorimetry* **110**, 535 (2012)
19. M. Alcoutlabi and G.B. McKenna, *J. Phys. Condens.Matter***. 17**, 461 (2005).
20. Q. Jiang and X.Y. Lang, *Rapid Commun.* **25**, 825 (2004).
21. A. Attili, P.Gallo and M. Rovere, *Phys. Rev. E*. **71**, 031204 (2005).
22. G. Klose and H.J. Fecht, *Mater. Sci. Eng. A*. **180**, 77 (1994).
23. W.S. Saslow, *Phys. Rev. B*. **37**, 676 (1988).
24. W. Gao, M. Zhao and Q. Jiang, *J. Phys. Chem. C.* **111**, 4042 (2007).
25. J. R. Morones, J. L. Elechiguerra, A. Camacho, K. Holt, J. B. Kouri, J. T. Ramírez and M. J. Yacaman, *Nanotechnology.* **16**, 2346 (2005).
26. Y. Wang, Z. Cui, Z. Zhang. *Materials Letters.* **58**, 3017 (2004).
27. K. K. Nanda, S.N. Sahu, S.N. Behera, *Phys. Rev. A*. **66,** 13208 (2002).
28. G. Guisbiers, M. Wautelet, *Nanotechnology.* **17,** 2008 (2006).
29. A. Safaei, M. A. Shandiz, S. Sanjabi, Z. H. Barber, *J. Phys. Chem. C*. **112**, 99 (2008).
30. G. Guisbiers, M. Kazan, O. Van Overschelde, M. Wautelet, S. Pereira, *J. Phys. Chem. C*. **112**, 4097 (2008).
31. R. Kumar and M. Kumar, *Indian J. Pure Appl. Phys.* **50**, 329 (2012).

32. G. Guisbiers, *Nanoscale Res. Lett.* **5**, 1132 (2010).
33. S. Bhatt, M. Kumar, *J. of Phys. Chem. Solids.* **106**, 112 (2017).
34. W.H. Qi , *Physica B.* **368**, 46 (2005).
35. Y. Z. Li et al., *J. Chem. Phys.* **146**, 224502 (2017).
36. X. Zhang et al., *J. Phys.: Condens. Matter*. **31**, 7 (2018).
37. S. Lampman, *Characterization and Failure Analysis of Plastics, ASM International.*, 115 (2003).
38. H. M. Lu, P. Y. Li, Z. H. Cao, X. K. Meng, *J. Phys. Chem. C.* **113**, 7598 (2009).